Photoluminescence and contactless electroreflectance characterization of $Be_xCd_{1-x}Se$ alloys

2007 J. Phys.: Condens. Matter 19 026208

(http://iopscience.iop.org/0953-8984/19/2/026208)

INSTITUTE OF PHYSICS PUBLISHING JOURNAL OF PHYSICS: CONDENSED MATTER

J. Phys.: Condens. Matter **19** (2007) 026208 (11pp) doi:10.1088/0953-8984/19/2/026208

Photoluminescence and contactless electroreflectance characterization of $Be_xCd_{1-x}Se$ alloys

P J Huang[1], Y S Huang[1,5], F Firszt[2], H Męczyńska[2], O Maksimov[3], M C Tamargo[3] and K K Tiong[4]

[1] Department of Electronic Engineering, National Taiwan University of Science and Technology, Taipei 106, Taiwan
[2] Institute of Physics, N Copernicus University, Grudziądzka 5/7, 87-100 Toruń, Poland
[3] New York State Center for Advanced Technology on Ultrafast Photonics, Center for Analysis of Structures and Interfaces, and Department of Chemistry, City College of the City University of New York, New York, NY 10031, USA
[4] Department of Electrical Engineering, National Taiwan Ocean University, Keelung 202, Taiwan

E-mail: ysh@mail.ntust.edu.tw

Received 3 November 2006
Published 15 December 2006
Online at stacks.iop.org/JPhysCM/19/026208

Abstract

A detailed optical characterization of a Bridgman-grown wurtzite- (WZ-) type $Be_{0.075}Cd_{0.925}Se$ mixed crystal and three zinc-blende (ZB) $Be_xCd_{1-x}Se$ epilayers grown by MBE on InP substrates has been carried out via photoluminescence (PL) and contactless electroreflectance (CER) in the temperature range of 15–400 K. The PL spectrum of the WZ-BeCdSe at low temperature consists of an exciton line, an edge emission feature due to recombination of donor–acceptor pairs, and a broad band related to recombination through deep-level defects, while the PL emission peaks of the ZB-BeCdSe epilayers show an asymmetric shape with a tail on the low-energy side. Various interband transitions, originating from the band edge and spin–orbit splitting critical points, of the samples have been observed in the CER spectra. The peak positions of the exciton emission lines in the PL spectra correspond quite well to the energies of the fundamental transitions determined from electromodulation data. The parameters that describe the temperature dependence of the fundamental and spin split-off bandgaps and the broadening function of the band-edge exciton are evaluated and discussed.

1. Introduction

Wide bandgap II–VI compounds are currently under investigation because of their possible applications in optoelectronic devices [1]. The applications include the use of II–VI compound based materials as light sources, in full colour displays and for increasing the information

[5] Author to whom any correspondence should be addressed.

density in optical recording [2, 3]. According to theoretical prediction and subsequent experimental verification, the beryllium containing II–VI compounds had been found to possess an enhanced ability to significantly reduce the defect propagation due to a greater prevalence of strong covalent bonding and lattice hardening in the materials [4, 5]. The strong covalent bonding in beryllium-based II–VI compounds achieves a considerable lattice hardening, which avoids multiplication of defects during the operation of II–VI semiconductor laser devices [6, 7]. $Be_xCd_{1-x}Se$ alloys have attracted great attention because they are promising for the fabrication of full-colour visible optical devices due to a large difference in the energy gaps E_g of the binary constituents (CdSe, $E_g = 1.74$ eV; BeSe, $E_g = 5.5$ eV) [8] and they seem to offer some alternative device structures to those based on ZnSe. It was recently proposed as an active region material in the blue–green laser diode and visible light-emitting diodes. In spite of their potential applications, very little work has been done on these compounds. Some studies have been performed for thin layers of zinc-blende (ZB) $Be_xCd_{1-x}Se$ [8, 9], but the basic properties of bulk $Be_xCd_{1-x}Se$ alloys are only little known due to the difficulties in growing high-quality samples.

In this work we present a detailed characterization of a Bridgman-grown wurtzite- (WZ-) type $Be_{0.075}Cd_{0.925}Se$ mixed crystal and three zinc-blende- (ZB-) type $Be_xCd_{1-x}Se$ epilayers grown on InP substrates by molecular-beam epitaxy (MBE) using photoluminescence (PL) and contactless electroreflectance (CER) in the temperature range between 15 and 400 K. PL spectra at low temperature consist of a band-edge exciton line and defect related emission bands. The peak positions of the exciton emission lines in the PL spectra correspond quite well to the energies of the fundamental transitions determined from electromodulation data. The parameters that describe the temperature dependence of the fundamental and spin split-off bandgaps and the broadening function of the band-edge exciton are evaluated and discussed.

2. Experimental details

In this study a WZ-$Be_{0.075}Ce_{0.925}Se$ mixed crystal and three ZB-$Be_xCd_{1-x}Se$ epilayers with different Be contents grown on InP substrates were measured. The WZ-type $Be_{0.075}Cd_{0.925}Se$ mixed crystal (sample I) was grown by the modified high pressure Bridgman method [10]. A chemically stable ingot with a nominal Be content $x = 0.075$ was cut into several 1–1.5 mm thick plates, mechanically polished and chemically etched. X-ray investigations show the crystal plates are uniform in composition and exhibit a single wurtzite phase or wurtzite as the main phase with admixture of another unidentified polytype. The ZB-$Be_xCd_{1-x}Se$ epilayers samples were grown on semi-insulating epiready InP(100) substrates using elemental Be, Cd and Se sources in a Riber 2300P MBE system. This system consists of III–V and II–VI growth chambers that are connected by an ultrahigh vacuum transfer channel. The substrates are deoxidized in the III–V chamber by heating to 480 °C with an As flux impinging on the InP surface. A lattice-matched InGaAs buffer layer (170 nm) was grown after the deoxidization. The samples were then transferred to the II–VI chamber for the growth of the BeCdSe epilayers. Prior to the initiation of the II–VI growth, the samples were heated to 170 °C and the III–V surface was exposed to a Zn flux for 30 s (Zn irradiation). Zn irradiation was followed by the growth of 10 nm of a low-temperature (170 °C) lattice-matched ZnCdSe interfacial layer. Growth of the BeCdSe layers was performed at 270 °C under Se-rich conditions. The BeCdSe alloy composition was controlled by adjusting the Be cell temperature and keeping the Cd flux constant. The growth rate was 0.4–0.6 μm h^{-1}. The Be composition of the three samples were determined to be 0.09, 0.14 and 0.20, and denoted as samples II, III and IV, respectively.

PL spectra were excited using the 325 nm line (∼55 mW) of a He–Cd laser. The luminescence signals were analysed by a Spex 0.85 m double spectrometer and detected by

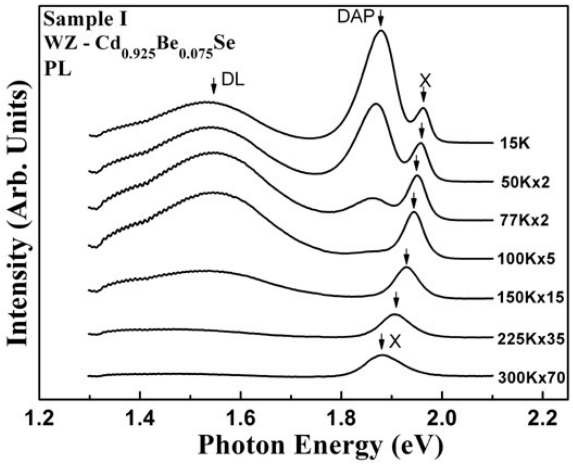

Figure 1. PL spectra of a WZ-$Be_{0.075}Ce_{0.925}Se$ mixed crystal (sample I) at several temperatures between 15 and 300 K.

a Hamamatsu photomultiplier tube. In CER an ac modulating voltage (∼1 kV at 200 Hz) is applied between a front wire grid electrode and a second electrode consisting of a metal plate. These two electrodes are separated by an insulating spacer in such a manner that there is a very thin layer (∼0.1 mm) of air (or vacuum) between the front surface of the sample and the front electrode. Thus, there is no direct contact with the front surface of the sample. The probe beam enters through the front wire grid. The radiation from a 150 W xenon arc lamp filtered by a 0.25 m monochromator provided the monochromatic light. The reflected light was detected by an UV-enhanced silicon photodiode. The dc output of this silicon photodiode was maintained constant by a servo mechanism of a variable neutral density filter. A dual-phase lock-in amplifier was used to measure the detected signals. For temperature dependent measurements, an RMC model 22 closed-cycle cryogenic refrigerator equipped with a digital thermometer controller was used for the low-temperature measurements. For the high-temperature experiments, each sample was mounted on one side of a copper finger of an electrical heater, which enabled one to control and stabilize the sample temperature. The temperature-dependent measurements were made between 15 and 400 K with the temperature stability of 0.5 K or better.

3. Results and discussion

Figure 1 shows the PL spectra of a WZ-$Be_{0.075}Ce_{0.925}Se$ mixed crystal (sample I) between 15 and 300 K. At 15 K, the PL spectrum consists of a sharp peak followed by a broader emission feature at an energy of about 95 meV lower than the first peak and a broad band in the energy range 1.5–1.7 eV. The broad band has been attributed to recombination through deep level defects [11]. As shown in figure 1 the first peak shifts monotonically towards lower energy with a broadened line shape character with increasing temperature in the range from 15 to 300 K, while the second feature is completely thermally quenched at temperature higher than 100 K. To examine the origin of these two near-band-edge luminescence features, the excitation intensity dependent PL measurements were carried out at 15 K. A linear dependence with a slope near unity was obtained for the first peak and no shift of the emission energy as a function of the excitation laser density was observed. The results indicate that this luminescence line is dominated by excitonic radiative recombination and denoted as X. In contrast, the second

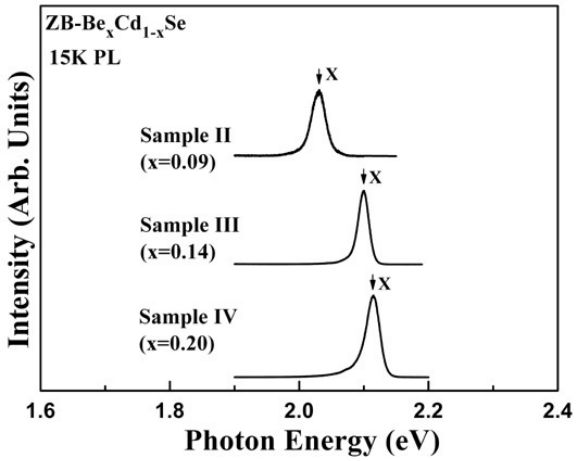

Figure 2. PL spectra of three ZB-$Be_xCd_{1-x}Se$ epilayer samples: $Be_{0.09}Cd_{0.91}Se$ (sample II), $Be_{0.14}Cd_{0.86}Se$ (sample III), and $Be_{0.20}Cd_{0.80}Se$ (sample IV) at 15 K.

emission band shifts towards higher photon energies with increasing intensity of exciting radiation. Taking into account the higher-energy shift with increasing excitation intensity as well as the thermal quenching, the second broader feature is interpreted to be an 'edge emission' due to recombination of donor–acceptor pairs.

Figure 2 illustrates the PL spectra of three ZB-$Be_xCd_{1-x}Se$ epilayer samples: $Be_{0.09}Cd_{0.91}Se$ (sample II), $Be_{0.14}Cd_{0.86}Se$ (sample III), and $Be_{0.20}Cd_{0.80}Se$ (sample IV) at 15 K. The PL emission peaks have an asymmetric shape with a tail at the low energy side. A similar asymmetric shape was previously observed for the ZnCdMgSe band-edge emission peaks [12]. In that case, it was suggested that the asymmetric ZnCdMgSe band-edge emission feature was a sum of a narrow free exciton recombination peak and a broad emission peak related to the recombination of excitons localized in the broad band tail by one longitudinal phonon energy [12]. The peak positions of the PL spectra show a blue-shift in the transition energy with the increase in Be content. The temperature evolutions (15–300 K) of near-band-edge PL spectra for the three samples are plotted in figures 3(a)–(c), respectively. As shown in figure 3, like the general property of most semiconductors, when the temperature is increased, the excitonic transitions in the PL spectra exhibit a red-shift and lineshape broadening characteristics. The lineshape broadening of the features is mainly due to the increase of exciton–phonon interaction effects.

The dotted curves in figures 4(a)–(d) represent, respectively, the experimental CER spectra of a WZ-$Be_{0.075}Ce_{0.925}Se$ mixed crystal (sample I), and three ZB-$Be_xCd_{1-x}Se$ epilayer samples: $Be_{0.09}Cd_{0.91}Se$ (sample II), $Be_{0.14}Cd_{0.86}Se$ (sample III), and $Be_{0.20}Cd_{0.80}Se$ (sample IV) at 15, 77, 150, 300, and 400 K. The full curves are least-squares fits to the first derivative of a Lorentzian lineshape (FDLL) function of the form [13, 14]

$$\frac{\Delta R}{R} = \mathrm{Re}\sum_{j=1} A_j\, \mathrm{e}^{\mathrm{i}\Phi_j}(E - E_j + \mathrm{i}\Gamma_j)^{-n} \tag{1}$$

where A_j and Φ_j are the amplitude and phase of the line shape, E_j and Γ_j are the energy and broadening parameter of the transitions, and the value of n depends on the origin of the transitions. For the first derivative functional form, $n = 2$ is appropriate for the bound states such as excitons [13].

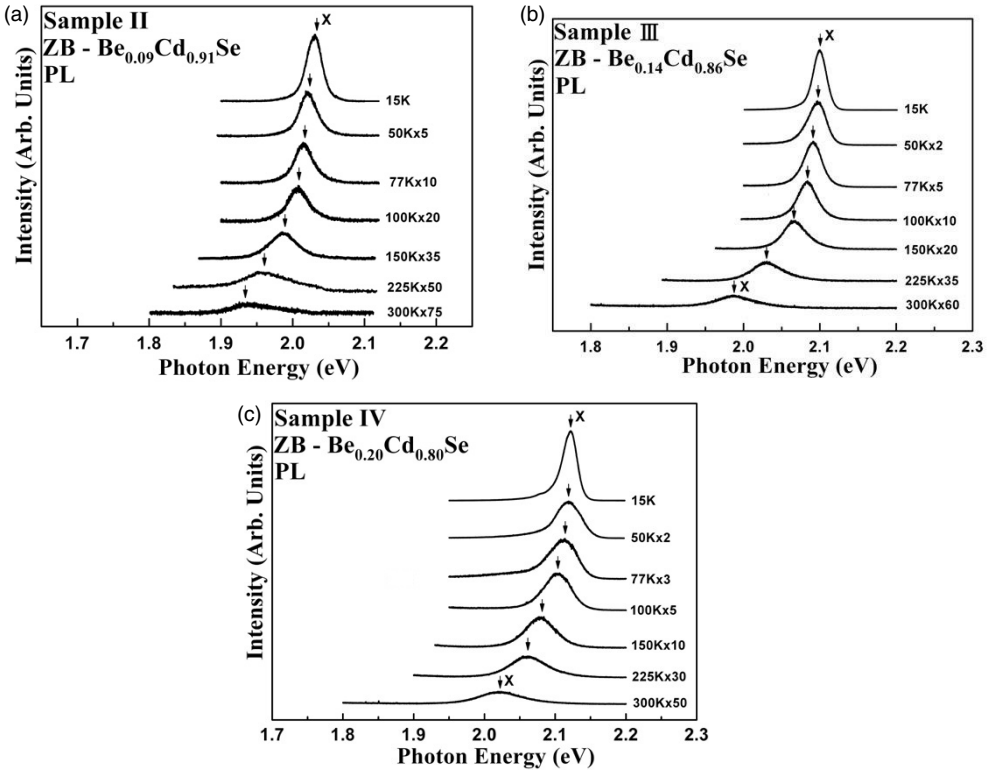

Figure 3. PL spectra of (a) $Be_{0.09}Cd_{0.91}Se$ (sample II), (b) $Be_{0.14}Cd_{0.86}Se$ (sample III), (c) $Be_{0.20}Cd_{0.80}Se$ (sample IV) at several temperatures between 15 and 300 K.

The CER spectrum of sample I, figure 4(a), at 15 K shows three distinct features as indicated by the vertical arrows. Their transition energies are determined to be 1.965 ± 0.003, 2.087 ± 0.003, and 2.398 ± 0.005 eV, respectively. As the temperature increases, the CER spectral features shift towards lower energies and broaden. The features on the lower-energy side are not clearly resolved at higher temperature. Nevertheless, lineshape fit reveals that two features are required to well describe the broadened structure at higher temperature. The fitted values of the transition energies at 300 K are 1.870 ± 0.004, 2.001 ± 0.004, and 2.305 ± 0.006 eV, respectively. The obtained values of the lowest transition feature at 1.965 eV (15 K) and 1.870 eV (300 K) agree quite well with the PL results of the band-edge exciton at 1.961 eV (15 K) and 1.865 eV (300 K). The value of 1.870 eV at 300 K also corresponds well to the transition energy of exciton A at 1.865 eV, as determined by Wronkowska *et al* [15] from the spectroscopic ellipsometry measurements performed at room temperature. They also reported the energy of exciton C to be 2.304 eV, which is nearly identical to the position of the highest energy feature for sample I. The work of Wronkowska *et al* [15] gives the energy separation of excitons A and C as 439 meV, which agrees well with the energy difference of 435 meV as evaluated from the present CER measurements for the lowest and the highest energy features. We can therefore assign the lowest energy feature to be exciton A and the highest energy feature to be exciton C. If we now turn our attention to the feature at 2.001 eV (300 K), denoted as Y, we find that the energy separation between this second feature and exciton A is ∼131 meV and is much larger than the room temperature energy difference between excitons A and B, ∼40 meV for WZ-CdSe [16]. Therefore, the assignment of the feature at 2.001 eV (300 K)

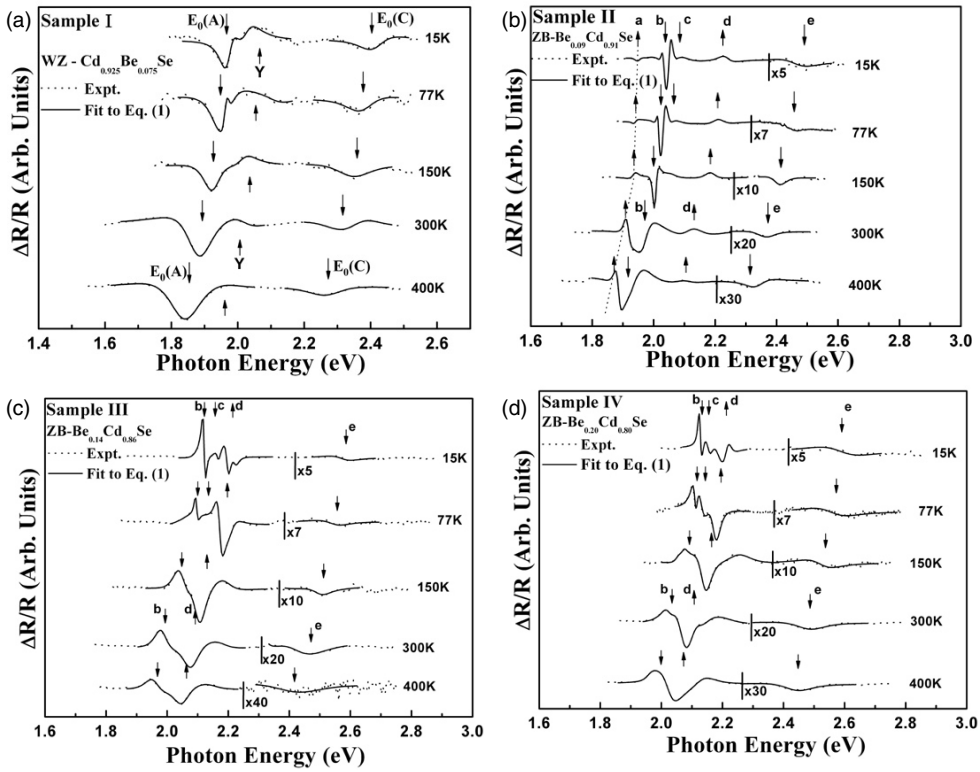

Figure 4. Experimental CER spectra (dotted curves) of (a) a WZ-$Be_{0.075}Ce_{0.925}Se$ mixed crystal (sample I), and three ZB-$Be_xCd_{1-x}Se$ epilayer samples: (b) $Be_{0.09}Cd_{0.91}Se$ (sample II), (c) $Be_{0.14}Cd_{0.86}Se$ (sample III), and (d) $Be_{0.20}Cd_{0.80}Se$ (sample IV) at 15, 77, 150, 300, and 400 K. The full lines are least-squares fits to equation (1). The obtained values of the energies are indicated by the arrows. The dashed line in (b) is a guide to the eye.

Table 1. The energy positions (in eV) of features ***b*–*e*** determined by fitting the CER spectra at 15 K for three ZB-$Be_xCd_{1-x}Se$ epilayers grown on InP substrates.

	Features			
Material	***b***	***c***	***d***	***e***
ZB-$Be_{0.09}Cd_{0.91}Se$	2.034 ± 0.002	2.060 ± 0.002	2.235 ± 0.003	2.459 ± 0.005
ZB-$Be_{0.14}Cd_{0.86}Se$	2.103 ± 0.002	2.126 ± 0.002	2.235 ± 0.003	2.533 ± 0.005
ZB-$Be_{0.20}Cd_{0.80}Se$	2.123 ± 0.002	2.141 ± 0.002	2.235 ± 0.003	2.560 ± 0.005

as exciton B may not be appropriate. The origin of this feature is not clear and is tentatively attributed to the coexistence of some other polytypic phases with wurtzite as the main phase in the Be-containing crystal.

The CER spectrum of sample II, figure 4(b), at 15 K shows five distinct features, denoted as ***a*–*e***, indicated by the vertical arrows, while for samples III and IV (figures 4(c) and (d)) only four features denoted as ***b*–*e*** are present. The energy positions for features ***b***, ***c***, ***d*** and ***e*** obtained from detailed lineshape fits using equation (1) are listed in table 1. Also from the fits, the energy position of the singular feature ***a*** appearing in figure 4(b) is determined to be 1.947 ± 0.002 eV. In general, as the temperature increases, the CER spectral features shift

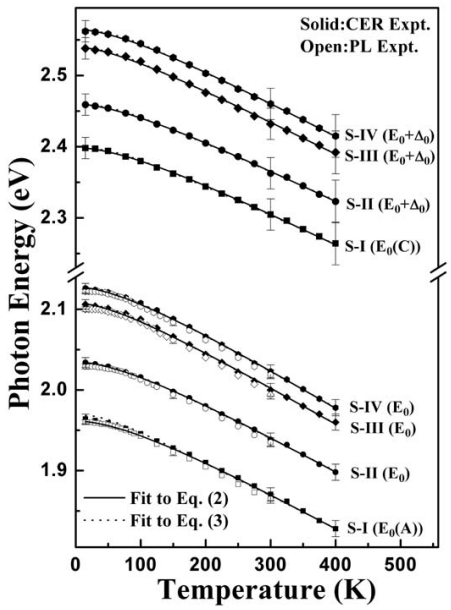

Figure 5. Temperature variations of the experimental CER values for $E_0(A)$ and $E_0(C)$ (solid squares) with representative error bars for sample I and temperature variations of the experimental CER values for E_0 and $E_0 + \Delta_0$ with representative error bars for samples II (solid circles), III (solid diamonds), and IV (solid hexagons). Open squares, circles, diamonds, and hexagons are the band-edge exciton peak positions in the PL spectra of samples I, II, III, and IV, respectively. The full curves are least-squares fits to equation (2) and the dotted lines are least-squares fits to equation (3).

towards lower energies and broaden. The rate of temperature redshift of feature ***a*** (shown as a dotted line in figure 4(b) for a guide to the eye) has been observed to be slower than the other four features as the temperature increases. This might indicate the origin of feature ***a*** to be different from other features and it is assigned as a defect-related transition. The origins of features ***b***–***e*** will be discussed as follows. The sharp doublet features ***b*** and ***c*** are quite similar to those of the excitonic transitions in ZnCdBeSe/InP examined by Hsieh *et al* [17]. The appearance of the doublets has been shown to be an indication of the heavy-hole (hh) and light-hole (lh) related excitonic transitions due to the existence of residual strain. As shown in table 1, the energy separations of features ***b*** and ***c*** decrease with the increase of Be content. This result might indicate that the residual strain of $Be_xCd_{1-x}Se/InP$ films decreases as the Be content increases from 0.09 to 0.20. It agrees quite well with the x-ray results [9]. At room temperature, the lattice mismatches are 1.76%, 0.92% and 0.01% for samples II, III and IV, respectively. The doublet features ***b*** and ***c*** are not clearly resolved at temperature higher than 150 K. Therefore, we fit the CER spectra with only three features for temperatures higher than 150 K. The origin of feature ***d*** is assigned as an interband transition of the ZnCdSe interfacial layer based on the similar energy position of the feature to the direct bandgap result of the previous CER study on $Zn_{0.56}Cd_{0.44}Se/InP$ by Malikova *et al* [18]. The energy separation of features ***b*** and ***e*** is evaluated to be ∼430 meV and is quite similar but slightly larger than the spin–orbital splitting $\Delta_0 = 410$ meV for cubic CdSe determined by spectroscopic ellipsometry measurements at room temperature [19]. We can therefore assign features ***b*** and ***e*** to be the band edge E_0 and its spin split-off $E_0 + \Delta_0$ transitions, respectively, for samples II, III and IV.

Plotted by the solid squares in figure 5 are the temperature variations of the experimental CER values for $E_0(A)$ and $E_0(C)$ with representative error bars for sample I. The temperature

Table 2. Values of $E(0)$, α, and β parameters obtained by fitting the band-edge excitonic transition energies with equation (2) and of a_B and Θ_B obtained from a least-squares fit with equation (3). The parameters for WZ-CdSe, $Cd_{0.92}Be_{0.08}Se/ZnCdMgSe$ (SQW), ZB-ZnSe, and ZB-$Zn_{0.56}Cd_{0.44}Se$ are included for comparison.

Samples	Feature	$E(0)$ (eV)	α (10^{-4} eV K^{-1})	β (K)	a_B (meV)	Θ_B (K)
WZ-$Be_{0.075}Cd_{0.925}Se$	X[a]	1.961 ± 0.003	4.53 ± 0.3	125 ± 30	29 ± 4	150 ± 30
	$E_0(A)$[a]	1.964 ± 0.003	4.02 ± 0.2	210 ± 20	34 ± 4	183 ± 30
	$E_0(C)$[a]	2.398 ± 0.005	3.92 ± 0.2	220 ± 30	38 ± 7	200 ± 30
ZB-$Be_{0.09}Cd_{0.91}Se$	X[a]	2.029 ± 0.003	4.65 ± 0.3	135 ± 30	31 ± 4	155 ± 30
	E_0[a]	2.034 ± 0.003	4.86 ± 0.3	200 ± 20	35 ± 4	175 ± 30
	$E_0 + \Delta_0$[a]	2.459 ± 0.005	4.78 ± 0.4	230 ± 30	40 ± 7	195 ± 30
ZB-$Be_{0.14}Cd_{0.86}Se$	X[a]	2.099 ± 0.003	5.26 ± 0.3	144 ± 30	34 ± 4	166 ± 30
	E_0[a]	2.106 ± 0.003	4.98 ± 0.3	208 ± 20	40 ± 4	188 ± 30
	$E_0 + \Delta_0$[a]	2.531 ± 0.005	5.10 ± 0.3	235 ± 30	44 ± 7	203 ± 30
ZB-$Be_{0.20}Cd_{0.80}Se$	X[a]	2.123 ± 0.003	5.45 ± 0.3	155 ± 30	38 ± 4	179 ± 30
	E_0[a]	2.126 ± 0.003	5.38 ± 0.3	210 ± 20	43 ± 4	195 ± 30
	$E_0 + \Delta_0$[a]	2.566 ± 0.005	5.41 ± 0.3	238 ± 30	48 ± 7	212 ± 30
WZ-CdSe[b]	$E_0(A)$	1.834 ± 0.003	4.24 ± 0.2	118 ± 40	36 ± 5	179 ± 40
	$E_0(B)$	1.860 ± 0.002	4.17 ± 0.1	93 ± 20	31 ± 6	152 ± 25
	$E_0(C)$	2.263 ± 0.004	3.96 ± 0.2	81 ± 35	27 ± 8	142 ± 40
$Cd_{0.92}Be_{0.08}Se/ZnCdMgSe$ (SQW)[c]	11H	2.079 ± 0.001	3.7 ± 0.3	249 ± 39	35 ± 2	210 ± 8
ZB-ZnSe[d]	E_0	2.800 ± 0.005	7.3 ± 0.4	295 ± 35	73 ± 4	260 ± 10
ZB-$Zn_{0.56}Cd_{0.44}Se$[d]	E_0	2.272 ± 0.004	6.1 ± 0.5	206 ± 35	62 ± 4	236 ± 10

[a] Present work (photoluminescence and contactless electroreflectance).
[b] Reference [16] (spectroscopic ellipsometry).
[c] Reference [21] (photoluminescence).
[d] Reference [18] (contactless electroreflectance).

variations of the experimental CER values for E_0 and $E_0 + \Delta_0$ with representative error bars for samples II, III, and IV are also depicted in figure 5 as solid circles, diamonds, and hexagons, respectively. For comparison purpose the band-edge excitonic peak positions in the PL spectra of samples I, II, III, and IV (open squares, circles, diamonds, and hexagons) are also displayed in figure 5 as well. It is noticed that the peak positions of band-edge exciton features in the PL spectra correspond quite well (slightly lower) to the fundamental transition energies of obtained from electromodulation data.

The full curve in figure 5 is a least-squares fit to the Varshni semi-empirical relationship [20] as given by equation (2),

$$E(T) = E(0) - \frac{\alpha T^2}{(\beta + T)}. \tag{2}$$

Here $E(0)$ is the energy at 0 K; α and β are constants. The constant α is related to the electron (exciton)–average phonon interaction and β is closely related to the Debye temperature [20]. The values obtained for $E(0)$, α, and β are listed in table 2. For comparison, the parameters for the near-band-edge transition energies of WZ-CdSe [16], CdBeSe/ZnCdMgSe (SQW) [21], ZB-ZnSe [18], and ZB-$Zn_{0.56}Cd_{0.44}Se$ [18] are also listed in table 2.

The temperature dependence of the peak positions of the band-edge exciton features can also be described by a Bose–Einstein-type expression [16]

$$E(T) = E(0) - 2a_B/[\exp(\Theta_B/T) - 1], \tag{3}$$

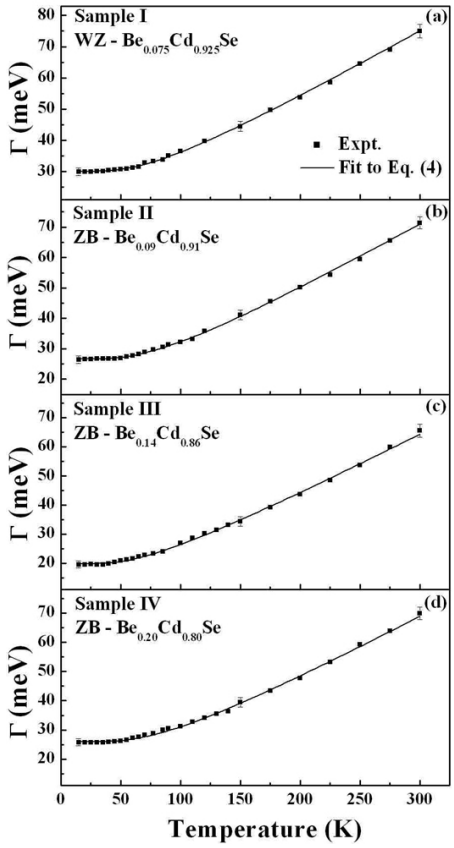

Figure 6. Experimental values of the temperature dependence of the linewidth $\Gamma(T)$ of the band-edge exciton features obtained by PL measurements for (a) sample I, (b) sample II, (c) sample III, and (d) sample IV, respectively, with representative error bars. The full curves are least-squares fits to equation (4).

where $E(0)$ is the transition energy at $T = 0$ K, a_B represents the strength of the electron (exciton)–average phonon interaction, and Θ_B corresponds to the average phonon temperature. Shown by the dotted lines in figure 5 is a least-squares fit to equation (3). The obtained values for the various parameters are also given in table 2. For comparison purposes, the parameters for the near-band-edge transition energies of WZ-CdSe [16], CdBeSe/ZnCdMgSe (SQW) [21], ZB-ZnSe [18], and ZB-$Zn_{0.56}Cd_{0.44}Se$ [18] are also listed in table 2.

The parameter α of equation (2) can be related to a_B and Θ_B in equation (3) by taking the high-temperature limit of both expressions. This yields $\alpha = 2a_B/\Theta_B$. Comparison of the numbers presented in table 2 shows that this relation is indeed satisfied. From equation (3), it is straightforward to show that the high temperature limit of the slope of the $E(T)$ versus T curve approaches a value of $-2a_B/\Theta_B$. The calculated value of $-2a_B/\Theta_B$ for the band-edge exciton is equal to -0.37, -0.39, -0.42, and -0.43 meV K^{-1} for samples I, II, III, and IV respectively, which agrees well with the value of $[dE_{A(0)}/dT] = -0.42$, -0.42, -0.43, and -0.44 meV K^{-1} as obtained from the linear extrapolation of the high-temperature (200–400 K) CER experimental data.

The experimental values of the temperature dependence of the linewidth $\Gamma(T)$ of the band-edge exciton features obtained by PL measurements are displayed in figures 6(a)–(d)

Table 3. Values of the parameters that describe the temperature dependence of the broadening function $\Gamma(T)$ for edge excitonic transitions of $Be_xCd_{1-x}Se$. The parameters for WZ-CdSe, $Cd_{0.92}Be_{0.08}Se$/ZnCdMgSe (SQW), ZB-ZnSe, and ZB-$Zn_{0.56}Cd_{0.44}Se$ are included for comparison.

Material	Feature	$\Gamma(0)$ (meV)	Γ_{LO} (meV)	Θ_{LO} (K)	γ_{AC} (μeV K^{-1})
WZ-$Be_{0.075}Cd_{0.925}Se$	E_0 (A)[a]	30 ± 2	42 ± 8	200 ± 80	3 ± 1
ZB-$Be_{0.09}Cd_{0.91}Se$	E_0[a]	26.6 ± 2	44 ± 8	210 ± 90	3 ± 1
ZB-$Be_{0.14}Cd_{0.86}Se$	E_0[a]	19.8 ± 2	47 ± 8	224 ± 90	3 ± 1
ZB-$Be_{0.20}Cd_{0.80}Se$	E_0[a]	26.1 ± 2	55 ± 8	246 ± 90	3 ± 1
WZ-CdSe[b]	$E_0(A)$ $E_0(C)$	2.3 ± 0.3 4 ± 1	23 ± 1 139 ± 25	300[c] 775 ± 86	
$Cd_{0.92}Be_{0.08}Se$/ZnCdMgSe (SQW)[d]	11H	23.3 ± 0.7	82 ± 16	300 ± 35	
ZB-ZnSe[e]	E_0	6.5 ± 2.5	24 ± 8	360[c]	2.0[c]
ZB-$Zn_{0.56}Cd_{0.44}Se$[e]	E_0	6.0 ± 2.0	17 ± 6	334[c]	1.1[c]

[a] Present work (photoluminescence).
[b] Reference [16] (spectroscopic ellipsometry).
[c] A fixed parameter.
[d] Reference [21] (photoluminescence).
[e] Reference [18] (contactless electroreflectance).

for samples I–IV, respectively. The temperature dependence of the linewidth of excitonic transitions of semiconductors can be expressed as [22]

$$\Gamma(T) = \Gamma(0) + \gamma_{AC}T + \frac{\Gamma_{LO}}{[\exp(\Theta_{LO}/T)]}. \tag{4}$$

In equation (4), $\Gamma(0)$ represents the broadening invoked from temperature-independent mechanisms, such as electron–electron interaction, impurity, dislocation, and alloy scattering, whereas the second term corresponds to lifetime broadening due to the exciton–acoustical phonon interaction with γ_{AC} being the acoustical phonon coupling constant. The third term is caused by the exciton–LO phonon (Fröhlich) interaction. The quantity Γ_{LO} represents the strength of the exciton–LO phonon coupling while Θ_{LO} is the LO phonon temperature [16, 23]. The full curves in figures 6(a)–(d) are least-squares fits to equation (4) to evaluate $\Gamma(0)$, Γ_{LO}, Θ_{LO}, and γ_{AC} for the band-edge exciton feature of samples I–IV respectively. The obtained values of $\Gamma(0)$, Γ_{LO}, Θ_{LO}, and γ_{AC} are listed in table 3. For comparison, the values of $\Gamma(0)$, Γ_{LO}, Θ_{LO}, and γ_{AC} for WZ-CdSe [16], CdBeSe/ZnCdMgSe (SQW) [21], ZB-ZnSe [18], and ZB-$Zn_{0.56}Cd_{0.44}Se$ [18] from other works are also included in table 3. The values of $\Gamma(0)$ for the Be-containing mixed crystal sample are much larger than those of Be-containing thin-film samples. Actually, it is not easy to grow high-quality Be-incorporated II–VI mixed crystal samples. It is also noticed that the values of Γ_{LO} and Θ_{LO} become larger with increasing Be content. The larger values of Γ_{LO} and Θ_{LO} are presumably related to the higher effective longitudinal optical phonon energy of the Be-containing samples.

4. Summary

In summary, we have studied the near-band-edge transitions of a modified Bridgman-grown wurtzite-type $Be_{0.075}Cd_{0.925}Se$ mixed crystal and a series of zinc-blende $Be_xCd_{1-x}Se$ epilayers grown by MBE on InP substrates has been investigated by PL and CER measurements in

the temperature range of 15 K $\leqslant T \leqslant$ 400 K. PL spectra at low temperatures consist of a sharp exciton line and broader features related to defects. The sharp band-edge excitonic feature in the PL spectra shows a blue-shift in the transition energy with the increase in Be content. Various interband transitions, originating from the band edge and spin–orbit splitting critical points, of the samples have been observed in the CER spectra. The peak positions of the exciton emission lines in the PL spectra correspond quite well to the energies of the fundamental transitions determined from electromodulation data. The temperature dependence of the fundamental and spin split-off bandgaps has been analysed by both Varshni- and Bose–Einstein-type expressions. The parameters extracted from both expressions by extending into the high-temperature regime are found to agree reasonably well. The parameters that describe the temperature dependence of the broadening function of the band-edge exciton have also been studied. The values of $\Gamma(0)$ for the Be-containing single-crystal sample are much larger than those of Be-containing thin-film samples. Actually, it is not easy to grow high-quality Be-containing II–VI single-crystal samples. The larger values of Γ_{LO} and Θ_{LO} are related to the higher effective longitudinal-optical-phonon energy of the Be-containing samples.

Acknowledgment

The authors PJH and YSH acknowledge the support of the National Science Council of Taiwan under project No NSC 95-2221-E-011-171.

References

[1] Klude M, Alexe G, Kruse C, Passow T, Heinke H and Hommel D 2002 *Phys. Status Solidi* b **229** 935
[2] Vigué F, Tournié E and Faurie J P 2000 *Appl. Phys. Lett.* **76** 242
[3] Bousquet V, Tournié E, Laugt M, Vennegues P and Faurie J P 1997 *Appl. Phys. Lett.* **70** 3564
[4] Wagg A, Fisher F, Schüll K, Baron T, Lugauer H J, Litz Th, Zehnder U, Ossau W, Gerhard T, Keim M, Reuscher G and Landwehr G 1997 *Appl. Phys. Lett.* **70** 280
[5] Zhang J Y, Shen D Z, Fan X W, Yang B J and Zhang Z H 2000 *J. Cryst. Growth* **214/215** 100
[6] Muñoz A, Rodríguez-Hernández P and Mujica A 1996 *Phys. Rev.* B **54** 11861
[7] Wagg A, Fisher F, Lugauer H J, Litz Th, Laubender J, Lunz U, Zehnder U, Ossau W, Gerhard T, Möller M and Landwehr G 1996 *J. Appl. Phys.* **80** 792
[8] Maksimov O, Guo S P and Tamargo M C 2002 *Phys. Status Solidi* b **229** 1005
[9] Maksimov O, Guo S P and Tamargo M C 2001 *Appl. Phys. Lett.* **78** 2473
[10] Firszt F, Łęgowski S, Męczyńska H, Szatkowski J, Paszkowicz W and Godwod K 2000 *J. Cryst. Growth* **184/185** 1335
[11] Mintairov A M, Raymond S, Merz J L, Peiris F C, Lee S, Bindley U, Furdyna J K, Melehin V G and Sadchikov K 1999 *Semiconductors* **33** 1021
[12] Zhou X, Gu Y, Kuskovsky Igor L, Neumark G F, Zeng L and Tamargo M C 2003 *J. Appl. Phys.* **94** 7136
[13] Pollak F H and Shen H 1993 *Mater. Sci. Eng.* R **10** 275
[14] Huang Y S and Pollak F H 2005 *Phys. Status Solidi* a **202** 1193
[15] Wronkowska A A, Wronkowski A, Firszt F, Łęgowski S, Męczyńska H, Marasek A and Paszkowicz W 2004 *Phys. Status Solidi* c **4** 641
[16] Logothetidis S, Cardona M, Lautenschlager P and Garriga M 1986 *Phys. Rev.* B **34** 2458
[17] Hsieh C H, Huang Y S, Ho C H, Tiong K K, Muñoz M, Maksimov O and Tamargo M C 2004 *Japan. J. Appl. Phys.* 1 **43** 459
[18] Malikova L, Krystek W, Pollak F H, Dai N, Cavus A and Tamargo M C 1996 *Phys. Rev.* B **54** 1819
[19] Janowitz C, Günther O, Jungk G, Johnson L, Santos P V, Cardona M, Faschinger W and Sitter H 1994 *Phys. Rev.* B **50** 2181
[20] Varshni Y P 1967 *Physica (Utrecht)* **34** 149
[21] Maksimov O, Guo S P, Muñoz M and Tamargo M C 2001 *J. Appl. Phys.* **90** 5135
[22] Lee J, Koteles E and Vassell M O 1986 *Phys. Rev.* B **33** 5512
[23] Lautenschlager P, Garriga M, Logothetidis S and Cardona M 1987 *Phys. Rev.* B **35** 9174